

Structural Evolution from Hyper-Honeycomb to Honeycomb Networks and Superconductivity in $\text{LaPt}_x\text{Si}_{2-x}$

Sitaram Ramakrishnan^{1*}, Tatsuya Yamakawa¹, Ryohei Oishi¹, Soichiro Yamane², Atsutoshi Ikeda², Masaki Kado¹, Yasuyuki Shimura¹, Toshiro Takabatake¹, Takahiro Onimaru¹, Yasuhiro Shibata³, Arumugam Thamizhavel⁴, Srinivasan Ramakrishnan⁵, Shingo Yonezawa², and Minoru Nohara^{1†}

¹ *Department of Quantum Matter, AdSE, Hiroshima University, Higashi-Hiroshima 739-8530, Japan*

² *Department of Electronic Science and Engineering, Graduate School of Engineering, Kyoto University, Kyoto 615-8510, Japan*

³ *Natural Science Center for Basic Research and Development, Hiroshima University, Higashi-Hiroshima 739-8526, Japan*

⁴ *Department of Condensed Matter Physics and Materials Science, Tata Institute of Fundamental Research, Mumbai 400005, India*

⁵ *Department of Physics, Indian Institute of Science Education and Research, Pune, 411008, India*

We report the crystal structures and superconductivity (SC) of $\text{LaPt}_x\text{Si}_{2-x}$ ($0.5 \leq x \leq 1.0$) that are solid solutions of LaSi_2 and LaPtSi with centrosymmetric tetragonal ($I4_1/amd$, D_{4h}^{19} , #141) and non-centrosymmetric tetragonal ($I4_1md$, C_{4v}^{11} , #109) structures, respectively. It was found that at $0.86 \leq x \leq 1.00$, the non-centrosymmetric tetragonal symmetry is preserved, while partial disorder appears in alternating Pt and Si of the hyper-honeycomb network. The superconducting transition temperature T_c was drastically reduced from 3.9 K to 1.5 K as x varies from 1.0 to 0.86. Additionally, a hexagonal phase with an AlB_2 -type structure ($P6/mmm$, D_{6h}^1 , #191) has been discovered at $0.50 \leq x \leq 0.71$ with a honeycomb network of statistically distributed Pt and Si atoms. The hexagonal phase exhibited SC at $T_c = 0.38$ K. This system provides an opportunity to investigate the relationship between topological electronic states, SC, and disorders.

1. Introduction

Equiatomic ternary silicide LaPtSi and isotypic compounds, such as LaNiSi , LaPtGe , and ThIrSi , are attracting considerable interest because the first-principles calculations suggest topological electronic states and exotic superconductivity (SC) due to their crystal structures with broken spatial inversion symmetry and nonsymmorphic space group.¹⁻³⁾ Additionally, muon-spin rotation and relaxation (μSR) measurements indicate topological SC with broken time-reversal symmetry (TRS) in LaNiSi , LaPtSi , and LaPtGe ,⁴⁾ while the TRS is preserved in ThIrSi .⁵⁾ These compounds crystallize into the non-centrosymmetric tetragonal structure of LaPtSi -type ($I4_1md$, C_{4v}^{11} , #109), which is an ordered vari-

*E-mail address: niranj002@gmail.com, Present address: I-HUB Quantum Technology Foundation, Indian Institute of Science Education and Research, Pune, 411008, India.

†E-mail address: mnohara@hiroshima-u.ac.jp

ant of the centrosymmetric tetragonal structure of α -ThSi₂-type ($I4_1/amd$, D_{4h}^{19} , #141). In LaSi₂ with α -ThSi₂-type structure, Si forms a hyper-honeycomb network characterized by three covalent bonds per Si in a twisted manner in a body-centered lattice, as depicted in Fig. 1(a). In contrast, in LaPtSi, the hyper-honeycomb network is formed by alternating Pt and Si atoms, thereby breaking the center of inversion, as depicted in Fig. 1(c), originally reported by Klepp and Parthé using powder X-ray diffraction (PXR).⁶⁾ Note that $I4_1md$ is a subgroup of $I4_1/amd$.

SC in the α -ThSi₂-type structure has been observed in the centrosymmetric compounds such as LaSi₂ with a superconducting transition temperature $T_c = 2.3$ K.⁷⁻¹⁴⁾ For the non-centrosymmetric counterpart, SC in LaPtSi was discovered at $T_c = 3.3$ K by Evers et al. through AC susceptibility measurements.¹⁵⁾ Ramakrishnan et al.¹⁶⁾ revealed that LaPtSi is a full-gap and weak-coupling *s*-wave superconductor in the dirty limit, where the T_c was comparatively higher at 3.9 K than the value reported by the earlier study.¹⁵⁾ Later, Kneidinger et al.¹⁷⁾ observed similar behavior in the SC of LaPtSi with a $T_c = 3.35$ K, close to that of Evers et al.¹⁵⁾ Furthermore, penetration depth measurements indicated dirty and full-gap *s*-wave SC in LaPtSi.¹⁸⁾ These observations suggest atomic disorders, which may impact possible topological band structures and SC in LaPtSi.

Atomic disorders are observed in α -ThSi₂-type solid solutions, ThRh_{*x*}Si_{2-*x*} and ThIr_{*x*}Si_{2-*x*}, which exhibit a large homogeneity range of $0 \leq x \leq 0.96$ and $0 \leq x \leq 1.0$, respectively.^{19,20)} Interestingly, T_c decreases from 3.2 K at $x = 0.0$ to below 1.7 K at $x \approx 0.25$, but reappears at $x > 0.7$ and reaches a maximum of 6.5 K at $x = 0.96$ and 1.0, respectively.^{19,20)} PXR inferred that Rh/Ir and Si were distributed statistically over the hyper-honeycomb network, making the system the α -ThSi₂-type structure.^{19,20)} However, Klepp and Parthé discussed the difficulty in determining atomic disorder from PXR in this class of compounds.⁶⁾ Braun mentioned that the T_c variation at $x > 0.7$ is rather suggestive of an atomic ordering phenomenon.²¹⁾ In other words, the LaPtSi-type structure, rather than the α -ThSi₂-type, is suggested at $x > 0.7$, although a question remains on the crystal structure transition from the α -ThSi₂-type to LaPtSi-type with x in ThRh_{*x*}Si_{2-*x*} and ThIr_{*x*}Si_{2-*x*}. It is interesting to note that for ThCo_{*x*}Si_{2-*x*} and ThNi_{*x*}Si_{2-*x*}, the hexagonal AlB₂-type structure ($P6/mmm$, D_{6h}^1 , #191) emerges at $x \approx 0.5$ in between the tetragonal α -ThSi₂-type phases at the smaller and larger x with miscibility gaps (phase separations) between them.^{22,23)}

In this paper, we report the assessment of crystal structures and SC in LaPt_{*x*}Si_{2-*x*} ($0.5 \leq x \leq 1.0$), solid solutions of LaSi₂ and LaPtSi with α -ThSi₂-type and LaPtSi-type structures, respectively. We grew a single crystal of LaPtSi by the Czochralski (Cz) method resulting in a crystal with composition LaPt_{0.88}Si_{1.12} and prepared polycrystalline samples of LaPt_{*x*}Si_{2-*x*} by arc melting with $x = 0.50, 0.75, 0.80, 0.85,$ and 1.00 . It is observed that the tetragonal LaPtSi-type structure remains undisturbed for the range of $0.86 \leq x \leq 1.00$ in LaPt_{*x*}Si_{2-*x*}, while the inter-site mixing of Pt and Si exists within the hyper-honeycomb network, confirmed by the refinement of single-crystal X-ray diffraction (SXRD) data on LaPt_{0.88}Si_{1.12}. The system exhibits a significant decrease in T_c from 3.9 K¹⁶⁾ at $x = 1.0$ to 1.5 K at $x = 0.86$, suggesting the effects of disorder on SC. By further reducing the Pt content x , a phase

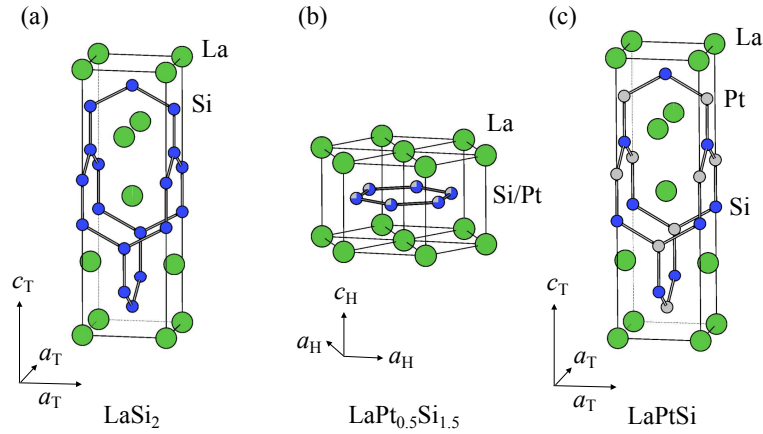


Fig. 1. (Color online) Crystal structures of three phases of $\text{LaPt}_x\text{Si}_{2-x}$. (a) LaSi_2 exhibits the tetragonal α - ThSi_2 -type structure ($I4_1/amd$, D_{4h}^{19} , #141). (b) $\text{LaPt}_{0.5}\text{Si}_{1.5}$ exhibits the hexagonal AlB_2 -type structure ($P6/mmm$, D_{6h}^1 , #191). (c) LaPtSi exhibits the tetragonal LaPtSi -type structure ($I4_1md$, C_{4v}^{11} , #109). In $\text{LaPt}_{0.5}\text{Si}_{1.5}$, Pt/Si forms a honeycomb network, while in LaSi_2 and LaPtSi , it forms a hyper honeycomb network. The structures are centrosymmetric in LaSi_2 and $\text{LaPt}_{0.5}\text{Si}_{1.5}$, while non-centrosymmetric in LaPtSi .

separation occurs, ultimately leading to the formation of a hexagonal AlB_2 -type phase ($P6/mmm$, D_{6h}^1 , #191) in $\text{LaPt}_x\text{Si}_{2-x}$ within the range of $0.50 \leq x \leq 0.71$. We have newly discovered that this hexagonal phase is also superconducting, albeit with a reduced T_c of 0.38 K at $x = 0.50$.

2. Experimental

A single crystal of $\text{LaPt}_{0.88}\text{Si}_{1.12}$ was grown using a modified Cz method. Polycrystalline samples of $\text{LaPt}_x\text{Si}_{2-x}$ with nominal compositions of $x = 0.50, 0.75, 0.80, 0.85,$ and 1.00 were synthesized by arc-melting. The composition of the samples was determined using an electron-probe microanalyzer (EPMA) (JXA-iSP100) with an accelerating voltage of 20 kV and a beam current of 30 nA. Hereafter, we denote nominal and analyzed values by x_{nominal} and x_{analyzed} , respectively. Further details of sample preparation are described in the Appendix.

SXRD was measured on a four-circle Bruker diffractometer employing Mo $K\alpha$ radiation for $\text{LaPt}_{0.88}\text{Si}_{1.12}$. SXRD data were processed by the APEX-III software.²⁴⁾ Structure refinements were done using JANA 2006.²⁵⁾ The results from SXRD are consistent with the composition determined by EPMA, resulting in $\text{LaPt}_{0.88}\text{Si}_{1.12}$. The crystallographic table of SXRD is given in the Appendix. PXRD was measured on a Rigaku MiniFlex600 with Cu $K\alpha$ radiation and the Rietveld refinement was done for $\text{LaPt}_x\text{Si}_{2-x}$ with $x = 0.50$ using FULLPROF software package.²⁶⁾

For single-crystalline $\text{LaPt}_{0.88}\text{Si}_{1.12}$, the electrical resistivity was measured by the standard DC four probe method in a Physical Property Measurement System (PPMS, Quantum Design, USA). The specific heat measurements were carried out in the PPMS with a ^3He refrigerator. A superconducting quantum interference device (SQUID) magnetometer (MPMS, Quantum Design, USA) was used

Table I. Chemical composition and crystal structure of $\text{LaPt}_x\text{Si}_{2-x}$. x_{nominal} represents the prescribed value of x , while x_{analyzed} is determined by EPMA. T and H denote the tetragonal LaPtSi-type ($I4_1md$, C_{4v}^{11} , #109) and the hexagonal AlB₂-type ($P6/mmm$, D_{6h}^1 , #191) structures, respectively.

x_{nominal}	x_{analyzed} (Structure)	Type
1.00	0.98(2) (T)	Polycrystal
1.00	0.88(3) (T)	Single crystal
0.85	0.708(5) (H) + 0.86(4) (T)	Polycrystal
0.80	0.692(4) (H) + 0.869(5) (T)	Polycrystal
0.75	0.691(4) (H) + 0.870(7) (T)	Polycrystal
0.50	0.493(9) (H)	Polycrystal

to measure magnetization M . For polycrystalline $\text{LaPt}_x\text{Si}_{2-x}$, the electrical resistivity was measured using the PPMS with an adiabatic demagnetization refrigerator (ADR). AC susceptibility measurements were carried out using a home-built susceptometer, which fits in the PPMS with ADR. Details regarding the instrumentation is described by Yonezawa et al.²⁷⁾

3. Results and discussion

3.1 Tetragonal and hexagonal phases in $\text{LaPt}_x\text{Si}_{2-x}$

Table I shows the analyzed composition for $\text{LaPt}_x\text{Si}_{2-x}$, where one observes that for $x_{\text{nominal}} = 1.00$ and 0.50 , the x_{analyzed} is relatively close to x_{nominal} . However, for $x_{\text{nominal}} = 0.75, 0.80,$ and 0.85 , there is a phase separation resulting in both hexagonal AlB₂-type and tetragonal LaPtSi-type phases, as confirmed by PXRD. Details of EPMA and PXRD are described in the Appendix and, respectively.

For single-crystalline $\text{LaPt}_{0.88}\text{Si}_{1.12}$ in the tetragonal phase, all diffraction maxima were indexed by a single unit cell with lattice parameters $a_T = 4.2441(2)$ Å and $c_T = 14.5264(2)$ Å, similar to the published unit cell of LaPtSi,^{6,16–18)} albeit with a slight reduction in volume. Table II shows the atomic coordinates for tetragonal $\text{LaPt}_{0.88}\text{Si}_{1.12}$. Figure 1(c) shows the crystal structure of LaPtSi, which is isostructural to $\text{LaPt}_{0.88}\text{Si}_{1.12}$. They are derivatives of the α -ThSi₂-type structure, like LaSi₂¹²⁾ or SrGe₂,²⁸⁾ where the Si/Ge atoms form a hyper-honeycomb network in a body-centered lattice, resulting in a centrosymmetric ($I4_1/amd$) structure, as shown in Fig. 1(a). In LaPtSi, 50% of the Si atoms are replaced by Pt, and the hyper-honeycomb network is formed by alternating Pt and Si atoms, thereby breaking the center of inversion and crystallizing into the non-centrosymmetric structure ($I4_1md$), which is a subgroup of $I4_1/amd$. For $\text{LaPt}_{0.88}\text{Si}_{1.12}$, the hyper-honeycomb network is formed by alternating Pt-rich and Si-rich sites, preserving $I4_1md$ symmetry, thereby the structure is the LaPtSi-type.

With further reduction of x down to 0.5 , we have discovered a hexagonal phase as indicated in Fig. 1(b). Figure 2 shows the PXRD pattern along with the Rietveld refinement for the hexagonal phase with lattice parameters $a_H = 4.13149(5)$ Å and $c_H = 4.39936(7)$ Å with the space group $P6/mmm$, revealing that $\text{LaPt}_{0.5}\text{Si}_{1.5}$ crystallizes into the hexagonal AlB₂-type structure.

The change from tetragonal to hexagonal structure is further illustrated by a phase diagram de-

Table II. Structural parameters for the tetragonal structure of crystal of $\text{LaPt}_{0.88}\text{Si}_{1.12}$ at 300 K. Given are the occupancy, the fractional coordinates x , y , z of the atoms, their anisotropic displacement parameters (ADPs) U_{ij} ($i, j = 1, 2, 3$), and the equivalent isotropic displacement parameter $U_{\text{iso}}^{\text{eq}}$. The off-diagonal elements U_{12} , U_{13} , and U_{23} are zero because all atoms in the crystal structure occupy the $4a$ Wyckoff positions. $R_F(\text{obs/all}) = 0.0311/0.0363$, no. of parameters is 15. Refinement method used: Least-squares on F . Space group: $I4_1md$, C_{4v}^{11} , # 109. Criterion of observability: $I < 3\sigma(I)$.

Atom	Occupancy	x	y	z	U_{11}	U_{22}	U_{33}	$U_{\text{iso}}^{\text{eq}}$
La	1	0	0	0	0.0086(18)	0.0050(19)	0.0098(19)	0.0078(11)
Pt	0.83(3)	0	0	0.5852(2)	0.0108(10)	0.0010(10)	0.0042(9)	0.0053(6)
Si _{Pt}	0.17	0	0	0.5852	0.0108	0.0010	0.0042	0.0053
Si	0.95(3)	0	0	0.4188(7)	0.014(6)	0.009(7)	0.008(6)	0.011(4)
Pt _{Si}	0.05	0	0	0.4188	0.014	0.009	0.008	0.011

picting the variation in lattice parameters, as shown in Fig. 3. It is obvious from Fig. 3, for $x \geq 0.86$ the system remains tetragonal LaPtSi -type phase. However, for x in the range of $0.71 < x < 0.86$, a clear phase separation has been observed through EPMA. PXRD patterns, EPMA images and a table describing the phase separation in detail are given in the Appendix and. Currently it is unclear what happens in the range $x < 0.5$. However, on comparison with a similar compound $\text{CePt}_x\text{Si}_{2-x}$,²⁹⁾ a phase separation between tetragonal α - ThSi_2 -type and hexagonal AlB_2 -type phases can be expected.

A honeycomb network is characterized by a lattice parameter a_{H} of the hexagonal structure. The corresponding length in a hyper-honeycomb network can be expressed by two parameters a_{T} and $c_{\text{T}}/2\sqrt{3}$ using tetragonal lattice parameters. In the LaPtSi phase, a_{T} is similar to $c_{\text{T}}/2\sqrt{3}$, while in the LaSi_2 , a_{T} is significantly larger than $c_{\text{T}}/2\sqrt{3}$, as shown in Fig. 3, suggesting the distortion of the hyper-honeycomb network is small in the LaPtSi phase. In addition, a_{H} at the phase boundary of the hexagonal AlB_2 -type phase is close to a_{T} and $c_{\text{T}}/2\sqrt{3}$ of the tetragonal LaPtSi -type phase. This suggests that despite there being no group-subgroup relation between $P6/mmm$ and $I4_1md$, the characteristic feature of the body-centered lattice in the tetragonal phase which is the hyper-honeycomb network of Pt/Si atoms allows a distortion toward a honeycomb network, thereby resembling the AlB_2 -type structure.

3.2 Phase diagram of superconductivity in $\text{LaPt}_x\text{Si}_{2-x}$

Figure 4 shows the results of magnetic measurements in $\text{LaPt}_x\text{Si}_{2-x}$. SC is observed at $T_{\text{c}} = 3.6$ and 2.2 K for $x = 1.00$ and 0.88, respectively, in the tetragonal LaPtSi -type phase, while $T_{\text{c}} = 0.38$ K for $x = 0.50$ in the hexagonal AlB_2 -type phase. For $x = 0.80$ and 0.75, two superconducting transitions are observed due to phase separation. SC with lower T_{c} is attributed to the hexagonal phase, while that with higher T_{c} is attributed to the tetragonal phase, based on changes in the real part of AC susceptibility V_y at T_{c} with respect to x . Figure 5 shows electrical resistivity for $\text{LaPt}_x\text{Si}_{2-x}$. Zero resistivity was observed at $T_{\text{c}} = 3.56$ and 2.05 K for $x = 1.0$ and 0.88 in the tetragonal phase,

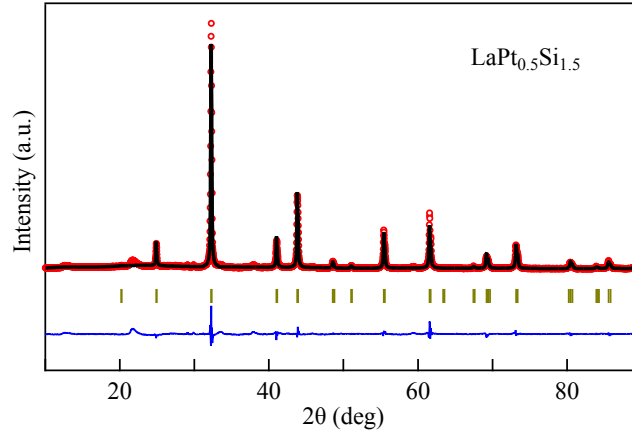


Fig. 2. (Color online) The PXR D pattern of $\text{LaPt}_{0.5}\text{Si}_{1.5}$ at room temperature. Red open circles, black and blue lines, and green bars indicate observed diffraction, fit, residual, and Bragg peak positions, respectively. The Rietveld refinement revealed a hexagonal structure, space group $P6/mmm$ (D_{6h}^1 , #191), lattice parameters $a_H = 4.13149(5)$ Å and $c_H = 4.39936(7)$ Å, and atomic positions of La at $1a$ (0, 0, 0), occupancy 1; Pt at $2d$ ($1/3$, $2/3$, $1/2$), occupancy 0.25; Si at $2d$ ($1/3$, $2/3$, $1/2$), occupancy 0.75. A good fit is obtained with Bragg $R_F = 5.55\%$ and $\chi^2 = 5.2101$.

respectively, while $T_c = 0.33$ K for $x = 0.50$ in the hexagonal phase. Resistivity exhibited the higher- T_c transitions for the phase separated samples ($x = 0.75, 0.80$, and 0.85). For $x = 0.50$, a superconducting volume of 60–70% is estimated from the change ΔV_y below T_c by comparing the superconducting transition of the Al standard.²⁷⁾

SC in hexagonal and tetragonal phases is further elucidated by a phase diagram depicting the change in T_c as a function of x_{analyzed} . From Fig. 6, it is evident that in the tetragonal phase, T_c decreases markedly with decreasing x_{analyzed} : $\text{LaPt}_{0.88}\text{Si}_{1.12}$ shows SC at 2.05 K, which is lower than the values of 3.9 K and 3.35 K reported for LaPtSi .^{16,17)} The smaller value of residual resistivity ratio (RRR) of 1.5 (as shown in the inset of Fig. 5), compared to earlier works,^{16,17)} suggests disorder in the present sample, which can be a possible origin of the reduced T_c . In contrast, the electronic specific-heat coefficient $\gamma = 8.11$ mJ/K²mol for the present $\text{LaPt}_{0.88}\text{Si}_{1.12}$ (as described later) is considerably larger than 3.56 mJ/K²mol and 6.5 mJ/K²mol for LaPtSi .^{16,17)} In the hexagonal phase, T_c depends weakly on x_{analyzed} .

3.3 Upper critical fields in $\text{LaPt}_{0.5}\text{Si}_{1.5}$ and $\text{LaPt}_{0.88}\text{Si}_{1.12}$

The superconducting transition temperature T_c decreases with magnetic field H in the hexagonal phase of $\text{LaPt}_{0.5}\text{Si}_{1.5}$ and the tetragonal phase of $\text{LaPt}_{0.88}\text{Si}_{1.12}$, as shown in Figs. 7(a) and 7(b), respectively. We defined the transition temperature $T_c(H)$ at the temperature where resistivity reaches 50% of the residual resistivity, and the upper critical field $H_{c2}(T)$ was plotted against temperature T in Fig. 7(c). Linear fits gave estimates of $\mu_0 H_{c2}(0) = 0.19$ and 1.1 T for $\text{LaPt}_{0.5}\text{Si}_{1.5}$ and $\text{LaPt}_{0.88}\text{Si}_{1.12}$, respectively.

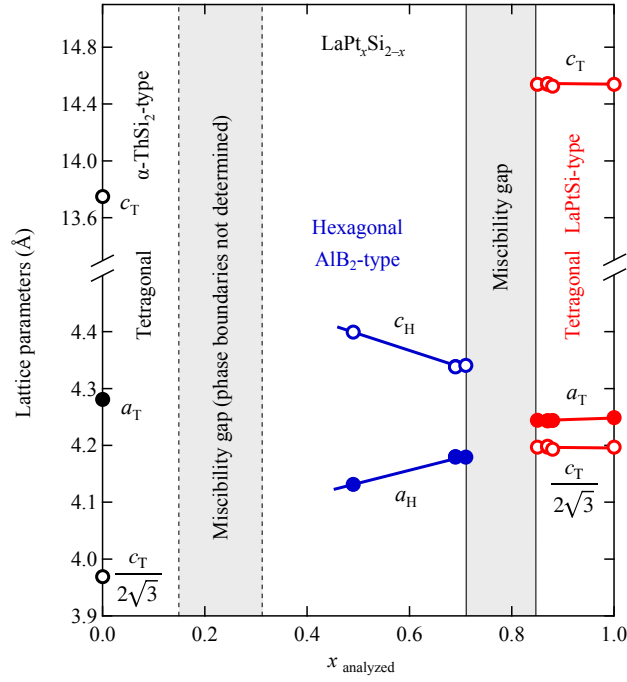


Fig. 3. (Color online) Structural phase diagram of $\text{LaPt}_x\text{Si}_{2-x}$. Lattice parameters are plotted as a function of x_{analyzed} , which was determined by EPMA. a_T and c_T denote lattice parameters of the tetragonal structures, while a_H and c_H denote lattice parameters of the hexagonal structure. $c_T/2\sqrt{3}$ is plotted to compare with a_T to characterize the hyper-honeycomb network. At $x \geq 0.86$, the crystal structure is tetragonal LaPtSi-type ($I4_1md$, C_{4v}^{11} , #109). A separation of two phases is observed for $0.71 < x < 0.86$. Within the range of $0.50 \leq x \leq 0.71$, the crystal structure is hexagonal AlB_2 -type ($P6/mmm$, D_{6h}^1 , #191). Currently, it is not known what happens at $0 < x < 0.50$, perhaps there is yet another phase separation. At $x = 0.0$, the crystal structure is tetragonal $\alpha\text{-ThSi}_2$ -type structure ($I4_1/amd$, D_{4h}^{19} , #141).

Here, we compare $H_{c2}(0)$ with the Pauli limit H_P , which is given by $\mu_0 H_P \simeq 1.86T_c$. For $T_c = 0.33$ K and 2.2 K, the corresponding $\mu_0 H_P$ values are 0.61 T and 4.1 T for $\text{LaPt}_{0.5}\text{Si}_{1.5}$ and $\text{LaPt}_{0.88}\text{Si}_{1.12}$, respectively, which are significantly higher than the observed $H_{c2}(0)$. This indicates that the upper critical fields in these compounds are governed by the orbital limit. LaPtSi has also been reported to be in the orbital limit.^{16,17} In this context, our data suggest conventional s -wave superconductivity, indicating that exotic superconducting states, such as mixed spin-singlet and spin-triplet pairing, are not present in the non-centrosymmetric $\text{LaPt}_{0.88}\text{Si}_{1.12}$.

We emphasize the importance of investigating whether topological electronic states, such as Weyl nodal rings around X points¹⁾ and bulk Dirac points,²⁾ remain stable against site mixing, which is inevitable in $\text{LaPt}_x\text{Si}_{2-x}$, as demonstrated in the present study. Such an investigation is crucial for realizing topological superconductivity, which can emerge from the combination of topological electronic states and s -wave superconductivity.²⁾

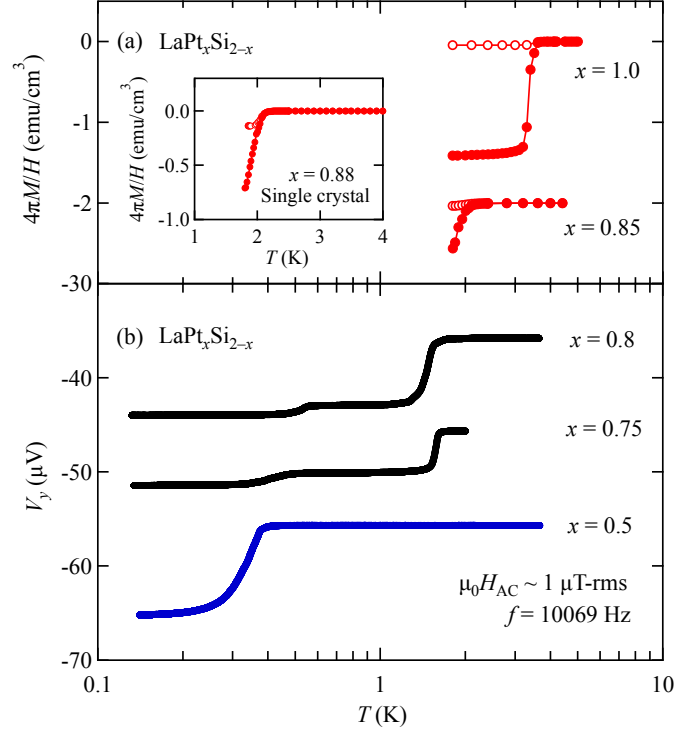


Fig. 4. (Color online) (a) Temperature dependence of the magnetization divided by field M/H of $\text{LaPt}_x\text{Si}_{2-x}$ with $x = 1.0$ and 0.85 in a field of 1 mT in the zero-field-cooled (ZFC) and field-cooled (FC) conditions. The inset shows M/H of single-crystalline $\text{LaPt}_x\text{Si}_{2-x}$ with $x = 0.88$. (b) Real part of AC magnetic susceptibility V_y of $\text{LaPt}_x\text{Si}_{2-x}$ with $x = 0.8, 0.75,$ and 0.50 . The data are shifted vertically for the sake of clarity.

3.4 Specific heat in $\text{LaPt}_{0.5}\text{Si}_{1.5}$ and $\text{LaPt}_{0.88}\text{Si}_{1.12}$

Figure 8 illustrates the specific heat divided by the temperature C/T as a function of the squared temperature T^2 for $\text{LaPt}_{0.5}\text{Si}_{1.5}$ in the hexagonal phase and $\text{LaPt}_{0.88}\text{Si}_{1.12}$ in the tetragonal phase. Normal-state data above T_c can be well-fitted by $C/T = \gamma + \beta T^2$, where γ represents the electronic specific heat coefficient and β represents the phonon contributions, from which the Debye temperature Θ_D is estimated. In the tetragonal phase of $\text{LaPt}_{0.88}\text{Si}_{1.12}$, a notable jump in specific heat occurs around 2.1 K , which corroborates the T_c determined from both magnetization and resistivity measurements. The ratio of this jump $\Delta C/\gamma T_c$ is calculated as 1.23 , with γ being $8.11 \text{ mJ/K}^2\text{mol}$, comparable to the value of the BCS weak coupling limit (1.43), indicating the bulk nature of SC. The Debye temperature Θ_D is estimated as 259 K from $\beta = 0.335 \text{ mJ/K}^4\text{mol}$, using the equation $\Theta_D = (12NR\pi^4/5\beta)^{1/3}$, where N represents the number of atoms in the formula and R denotes the gas constant. In the hexagonal phase of $\text{LaPt}_{0.5}\text{Si}_{1.5}$, γ is estimated as $4.42 \text{ mJ/K}^2\text{mol}$, β as $0.132 \text{ mJ/K}^4\text{mol}$, and $\Theta_D = 353 \text{ K}$. Since SC occurs at a much lower temperature of 0.38 K for this phase, our experimental setup did not allow us to observe the jump at even lower temperatures. However, the AC susceptibility indicates the bulk nature of SC.

One can estimate thermodynamic critical field $H_c(0)$ at $T = 0 \text{ K}$ using γ and T_c values from the

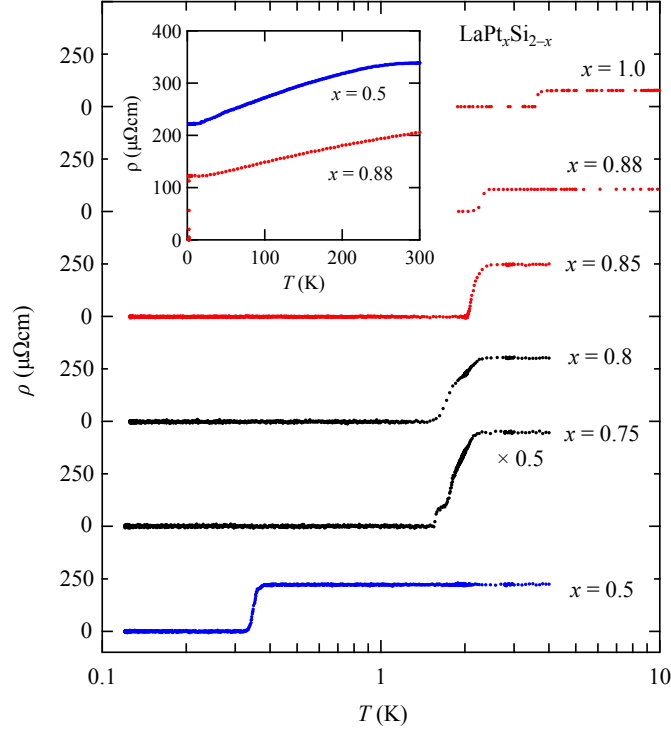


Fig. 5. (Color online) Temperature dependence of the electrical resistivity ρ for polycrystalline $\text{LaPt}_x\text{Si}_{2-x}$ at nominal values of $x = 1.0, 0.85, 0.80, 0.75,$ and 0.50 , as well as for a single crystal of $\text{LaPt}_x\text{Si}_{2-x}$ with an analyzed value of $x = 0.88$. The inset shows ρ for $x = 0.88$ (single crystal) and 0.50 (poly crystal) over a wide temperature range.

ratio of $H_c(0)^2/\gamma T_c^2 = 5.94$ for the BCS weak coupling limit.³⁰⁾ Using the aforementioned values of γ and T_c , we estimated $\mu_0 H_c(0) = 2.87$ and 23.2 mT for $\text{LaPt}_{0.5}\text{Si}_{1.5}$ and $\text{LaPt}_{0.88}\text{Si}_{1.12}$, respectively. The Ginzburg-Landau parameter was estimated to be $\kappa = H_{c2}(0)/\sqrt{2}H_c(0) = 47$ and 33 for $\text{LaPt}_{0.5}\text{Si}_{1.5}$ and $\text{LaPt}_{0.88}\text{Si}_{1.12}$, respectively, which were larger than $1/\sqrt{2}$, indicating the type-II SC of both compounds. The Ginzburg-Landau coherence length was estimated to be $\xi_0 = 420$ and 170 Å for $\text{LaPt}_{0.5}\text{Si}_{1.5}$ and $\text{LaPt}_{0.88}\text{Si}_{1.12}$, respectively, using $\mu_0 H_c(0) = \Phi_0/2\pi\xi_0^2$, where Φ_0 is the magnetic flux quantum.

Figure 9 summarizes the dependence of T_c on Θ_D and γ for various compounds, including tetragonal LaPtSi -type compounds,^{16, 20, 31–33)} tetragonal α - ThSi_2 -type compounds,^{9, 20)} and hexagonal AlB_2 -type $\text{LaPt}_{0.5}\text{Si}_{1.5}$. From Fig. 9(a), it can be seen that lower values of Θ_D tend to correspond to higher values of T_c . ThIrSi exhibits the highest T_c and the lowest Θ_D among the LaPtSi -type compounds. This trend is also evident in the present $\text{LaPt}_x\text{Si}_{2-x}$ system: for LaPtSi and $\text{LaPt}_{0.88}\text{Si}_{1.12}$, a lower Θ_D corresponds to a higher T_c . Such a relationship between T_c and Θ_D has also been observed in other systems, such as $\text{BaNi}_2(\text{As}_{1-x}\text{P}_x)_2$ ³⁴⁾ and AEPd_2As_2 ($\text{AE} = \text{Ba}, \text{Sr}, \text{and Ca}$).³⁵⁾ In these systems, a lower Θ_D , which corresponds to low-lying phonons, results in a higher T_c due to strong electron-phonon coupling. The signature of strong coupling is evident in ThIrSi , as indicated by the enhanced specific heat

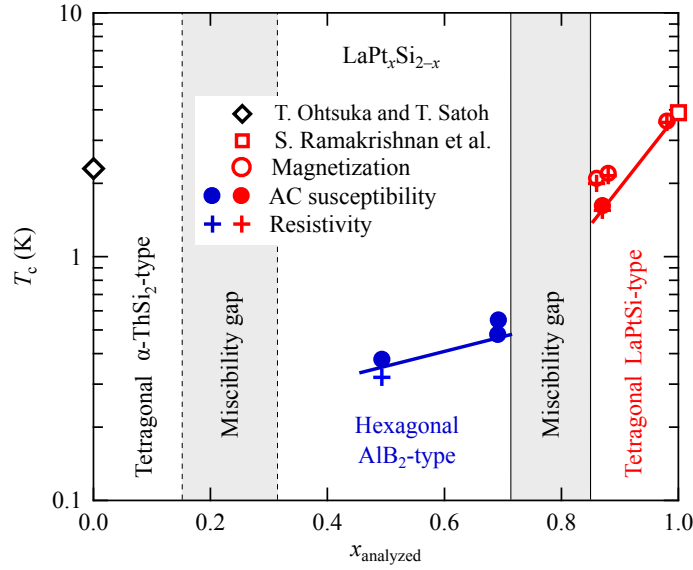


Fig. 6. (Color online) Relationship between the analyzed value of x and the superconducting transition temperature T_c in $\text{LaPt}_x\text{Si}_{2-x}$. The T_c values for LaSi_2 ($x = 0.0$) and LaPtSi ($x = 1.0$) are taken from T. Ohtsuka and T. Satoh,⁹⁾ and S. Ramakrishnan et al.,¹⁶⁾ respectively, and were determined from specific heat measurements.

jump $\Delta C/\gamma T_c = 4.73$,²⁰⁾ which is significantly larger than the BCS weak-coupling limit of 1.43. In contrast, the specific heat jump for the present $\text{LaPt}_{0.88}\text{Si}_{1.12}$ is close to the BCS weak-coupling limit, as mentioned above. Figure 9(b) shows the plot of T_c versus γ , which reveals an unusual trend: smaller γ values correspond to higher T_c . This is contrary to the typical trend in phonon-mediated superconductors, where a higher electronic density of states (DOS) at the Fermi level E_F , and thus a larger γ , is associated with a higher T_c .³⁶⁾ This suggests that in the family of LaPtSi -type compounds, the key factor determining T_c is not the electronic DOS at E_F , but rather the phonon properties, particularly the Debye temperature (Θ_D). This is consistent with theoretical calculations of the electron-phonon coupling constant and T_c .¹⁾ Zhang et al. demonstrated that the strongest electron-phonon coupling in LaPtSi originates from a phonon mode associated with the Pt motion.¹⁾ Accordingly, the observed decrease in T_c with decreasing x from 1.0 to 0.86 in tetragonal $\text{LaPt}_x\text{Si}_{2-x}$ can be attributed to changes in this phonon mode, which is likely modified due to the partial occupation of the Pt site in the ordered hyper-honeycomb network, shown in Fig. 1(c), by Si atoms.

4. Conclusions

To summarize, we explored the crystal structures and superconductivity (SC) in the solid solutions of $\text{LaPt}_x\text{Si}_{2-x}$. We found that the site disorder (Pt/Si) in crystals of $\text{LaPt}_x\text{Si}_{2-x}$ significantly reduces the SC transition temperature in the non-centrosymmetric tetragonal phase, as compared to similar systems like $\text{ThRh}_x\text{Si}_{2-x}$ and $\text{ThIr}_x\text{Si}_{2-x}$.^{19,20)} Much like $\text{ThCo}_x\text{Si}_{2-x}$,²²⁾ a hexagonal phase

of an AlB_2 -type structure exists in $\text{LaPt}_x\text{Si}_{2-x}$ at around $x = 0.5$ between the centrosymmetric and non-centrosymmetric tetragonal phases. As seen from resistivity and susceptibility measurements, the hexagonal phase is also a superconductor with its T_c around 0.38 K. Such a discovery of a hexagonal phase with an AlB_2 -type structure within a small range of x has also been reported for $\text{ThCo}_x\text{Si}_{2-x}$, with an onset of SC around 2 K.²²⁾ SrSi_2 is another system that is a semiconductor in the cubic phase ($P4_132$, O^7 , #213); however, the partial substitution of Ni for Si results in a hexagonal phase of an AlB_2 -type structure, which is superconducting at 2.8 K.³⁷⁾ Our observation of a new superconductor, $\text{LaPt}_{0.5}\text{Si}_{1.5}$, in the hexagonal phase is an interesting addition to these families.

Acknowledgment

SXRD data was collected at SAIF laboratory, IIT Madras, India. EPMA was performed at NBARD, Hiroshima University, Japan (NBARD-00191). This work was supported by JSPS KAKENHI (Grant Nos. JP23H04630, JP23H04861, JP23H04870, JP22H01168, JP22K03529, JP22H04473, and JP21K03448), JGC-S Scholarship Foundation (No. 2010), The Hattori Hokokai Foundation (No. 21-010), and The Mazda Foundation (No. 21KK-191).

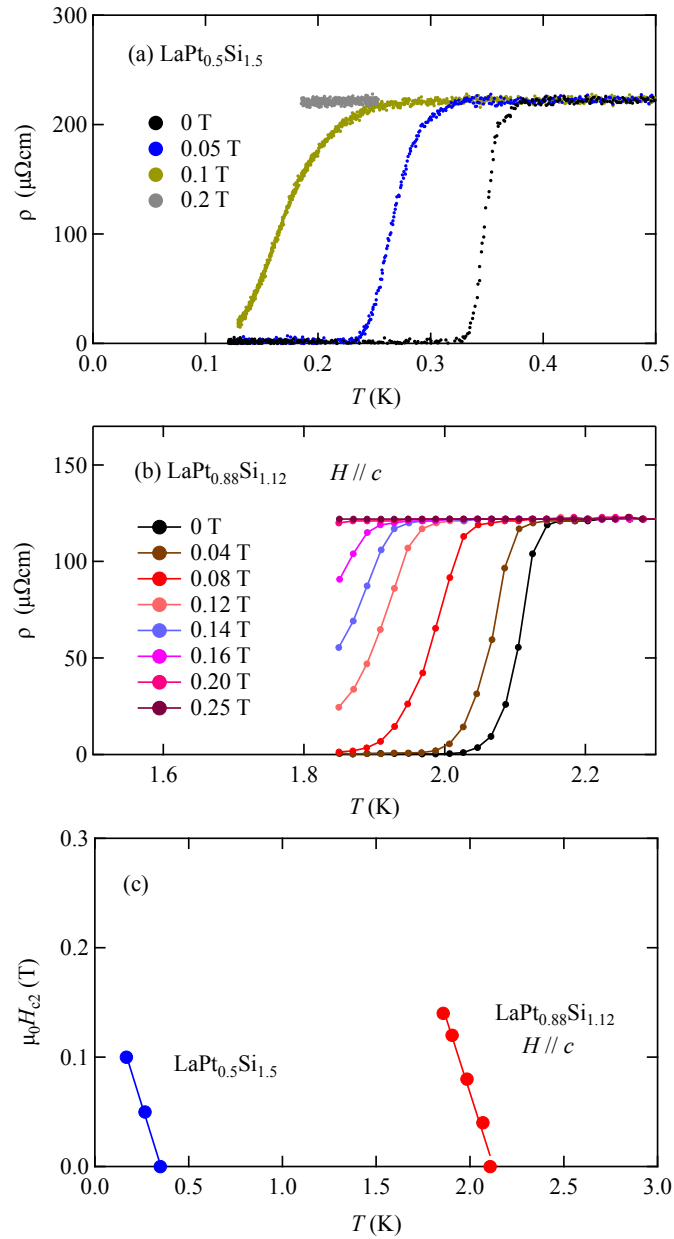


Fig. 7. (Color online) (a) The temperature dependence of the electrical resistivity of $\text{LaPt}_{0.5}\text{Si}_{1.5}$ in the hexagonal phase under various magnetic fields. (b) The temperature dependence of the electrical resistivity of single-crystalline $\text{LaPt}_{0.88}\text{Si}_{1.12}$ in the tetragonal phase under various magnetic fields. (c) The temperature dependence of the upper critical field H_{c2} of $\text{LaPt}_{0.5}\text{Si}_{1.5}$ and $\text{LaPt}_{0.88}\text{Si}_{1.12}$. The straight lines represent linear fits, from which we estimated $\mu_0 H_{c2}(0)$ to be 0.19 and 1.1 T for $\text{LaPt}_{0.5}\text{Si}_{1.5}$ and $\text{LaPt}_{0.88}\text{Si}_{1.12}$, respectively.

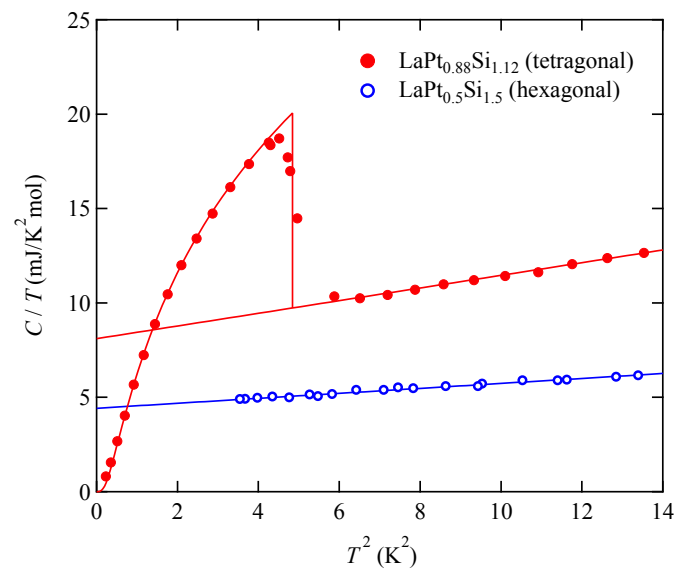


Fig. 8. (Color online) Specific heat divided by temperature, C/T , as a function of T^2 for LaPt_{0.88}Si_{1.12} (tetragonal phase) and LaPt_{0.5}Si_{1.5} (hexagonal phase). The straight lines represent fits by $C/T = \gamma + \beta T^2$, where γ is the electronic specific heat coefficient and β is a constant corresponding to the Debye phonon contributions.

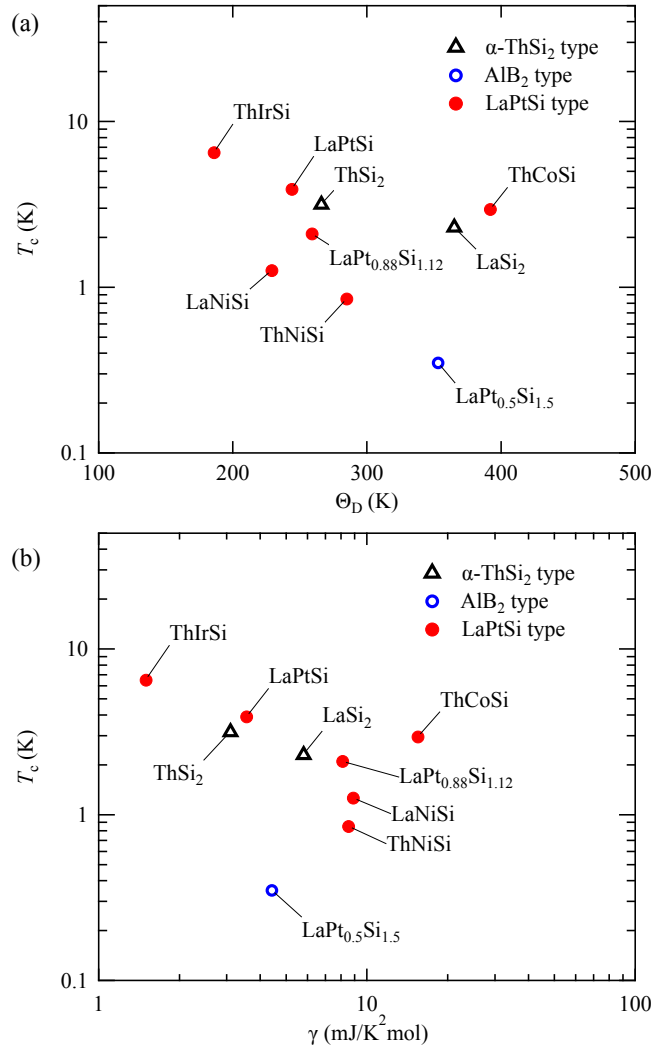


Fig. 9. (Color online) (a) Superconducting transition temperature T_c versus Debye temperature Θ_D , and (b) T_c versus the electronic specific heat coefficient γ for noncentrosymmetric LaPtSi-type (tetragonal, $I4_1md$) compounds: LaPtSi,¹⁶ ThIrSi,²⁰ ThCoSi,³¹ ThNiSi,³² LaNiSi,³³ and LaPt_{0.88}Si_{1.12} (present work); centrosymmetric α -ThSi₂-type (tetragonal, $I4_1/amd$) compounds: LaSi₂⁹ and ThSi₂,²⁰ and AlB₂-type (hexagonal, $P6/mmm$) LaPt_{0.5}Si_{1.5} (present work).

References

- 1) P. R. Zhang, H. Q. Yuan, and C. Cao, *Phys. Rev. B* **101**, 245145 (2020).
- 2) X. B. A. Shi, Q. B. Liu, P. He, Y. H. Yuan, X. P. Kong, K. Li, and W. W. Zhao, *Phys. Rev. B* **104**, 245129 (2021).
- 3) A. Ptok, K. Domieracki, K. J. Kapcia, J. Łazewski, P. T. Jochym, M. Sternik, P. Piekarczyk, and D. Kaczorowski, *Phys. Rev. B* **100**, 165130 (2019).
- 4) T. Shang, S. K. Ghosh, M. Smidman, D. J. Gawryluk, C. Baines, A. Wang, W. Xie, Y. Chen, M. O. Ajeesh, M. Nicklas, E. Pomjakushina, M. Medarde, M. Shi, J. F. Annett, H. Q. Yuan, J. Quintanilla, and T. Shiroka, *npj Quantum Materials* **7**, 35 (2022).
- 5) D. Tay, T. Shang, Priscila F. S. Rosa, F. B. Santos, J. D. Thompson, Z. Fisk, H.-R. Ott, and T. Shiroka, *Phys. Rev. B* **107**, 064507 (2023).
- 6) K. Klepp and E. Parthé, *Acta Crystallogr. Sect. B* **38**, 1105 (1982).
- 7) G. F. Hardy and J. K. Hulm, *Phys. Rev.* **93**, 1004 (1954).
- 8) B. T. Matthias, E. Corenzwit, and W. H. Zachariasen, *Phys. Rev.* **112**, 89 (1958).
- 9) T. Ohtsuka and T. Satoh, *Ann. Acad. Sci. Fennicæ Ser. A, VI. Physica* **210**, 92 (1966).
- 10) T. Satoh and T. Ohtsuka, *Phys. Lett.* **20**, 565 (1966).
- 11) D. McWhan, V. Compton, M. Silverman, and J. Soulen, *J. Less-Common Met.* **12**, 75 (1967).
- 12) T. Satoh and Y. Asada, *J. Phys. Soc. Jpn.* **28**, 263 (1970).
- 13) J. Evers, G. Oehlinger, and H. Ott, *J. Less-Common Met.* **69**, 389 (1980).
- 14) A. Iyo, I. Hase, K. Kawashima, S. Ishida, H. Kito, N. Takeshita, K. Oka, H. Fujihisa, Y. Gotoh, Y. Yoshida, and H. Eisaki, *Inorg. Chem.* **56**, 8590 (2017).
- 15) J. Evers, G. Oehlinger, A. Weiss, and C. Probst, *Solid State Commun.* **50**, 61 (1984).
- 16) S. Ramakrishnan, K. Ghosh, A. D. Chinchure, V. R. Marathe, and G. Chandra, *Phys. Rev. B* **52**, 6784 (1995).
- 17) F. Kneidinger, H. Michor, A. Sidorenko, E. Bauer, I. Zeiringer, P. Rogl, C. Blaas-Schenner, D. Reith, and R. Podloucky, *Phys. Rev. B* **88**, 104508 (2013).
- 18) S. Palazzese, J. F. Landaeta, D. Subero, E. Bauer, and I. Bonalde, *J. Phys.: Condens. Matter* **30**, 255603 (2018).
- 19) P. Lejay, B. Chevalier, J. Etourneau, J. Tarascon, and P. Hagenmuller, *Mater. Res. Bull.* **18**, 67 (1983).
- 20) B. Chevalier, Wang Xian Zhong, B. Buffat, J. Etourneau, P. Hagenmuller, P. Lejay, L. Porte, Tran Minh Duc, M. Besnus, and J. Kappler, *Mater. Res. Bull.* **21**, 183 (1986).
- 21) H. F. Braun, *J. Less-Common Met.* **100**, 105 (1984).
- 22) W. X. Zhong, W. L. Ng, B. Chevalier, J. Etourneau, and P. Hagenmuller, *Mater. Res. Bull.* **20**, 1229 (1985).
- 23) J. H. Albering, R. Pöttgen, W. Jeitschko, R.-D. Hoffmann, B. Chevalier, and J. Etourneau, *J. Alloys Compd.* **206**, 133 (1994).
- 24) APEX-III (APEX III software, Bruker Axs Inc., Madison, WI 2013).
- 25) V. Petricek, M. Dusek, and L. Palatinus, *Z. Kristallogr.* **229**, 345 (2014).
- 26) J. Rodríguez-Carvajal, *Phys. B: Condens. Matter* **192**, 55 (1993).
- 27) S. Yonezawa, T. Higuchi, Y. Sugimoto, C. Sow, and Y. Maeno, *Rev. Sci. Instrum.* **86**, 093903 (2015).
- 28) A. Iyo, I. Hase, K. Kawashima, S. Ishida, H. Kito, N. Takeshita, K. Oka, H. Fujihisa, Y. Gotoh, Y. Yoshida, and H. Eisaki, *Inorg. Chem.* **56**, 8590 (2017).
- 29) A. Griбанov, Y. Seropegin, A. Tursina, O. Bodak, P. Rogl, and H. Noël, *J. Alloys Compd.* **383**, 286 (2004).

- 30) J. Padamsee, H. Neighbor and C. Shiffman, *J. Low Temp. Phys.* **12**, 387 (1973).
- 31) K. Domieracki and D. Kaczorowski, *J. Alloys Compd.* **688**, 206 (2016).
- 32) K. Domieracki and D. Kaczorowski, *J. Alloys Compd.* **731**, 64 (2018).
- 33) W. H. Lee, F. A. Yang, C. R. Shih, and H. D. Yang, *Phys. Rev. B* **50**, 6523 (1994).
- 34) K. Kudo, M. Takasuga, Y. Okamoto, Z. Hiroi, and M. Nohara, *Phys. Rev. Lett.* **109**, 097002 (2012).
- 35) K. Kudo, Y. Yamada, T. Takeuchi, T. Kimura, S. Ioka, G. Matsuo, Y. Kitahama, and M. Nohara, *J. Phys. Soc. Jpn.* **86**, 063704 (2017).
- 36) H. Takagi, M. Nohara, and R. J. Cava, *Physica B* **237-238**, 292 (1997).
- 37) S. Pyon, K. Kudo, and M. Nohara, *J. Phys. Soc. Jpn.* **81**, 023702 (2012).

Appendix A: Synthesis

Single crystal of $\text{LaPt}_{0.88}\text{Si}_{1.12}$ was synthesized by the Czochralski (Cz) method in a tetra-arc furnace (Techno Search Corporation, Japan) under ultra-pure Ar atmosphere, following an iterative process as depicted in Fig. A·1 (a). Initially, high-purity elements La:Pt:Si (99.99% for La and Pt, and 99.999% for Si) were taken in a stoichiometric ratio of 1:1:1, totaling 10 g, and melted repeatedly to ensure homogeneity. A polycrystalline seed crystal was then cut from this ingot for crystal growth. The polycrystalline seed was gently inserted into the molten solution and initially pulled at a rapid speed of about 90 mm/h. The melt temperature was adjusted to form a neck, and then the pulling speed was reduced to approximately 10 mm/h for the remainder of the growth process. A 70 mm long ingot was pulled with a diameter of 3–4 mm, as shown in Fig. A·1(b). Laue diffraction confirmed that the crystal exhibited good single crystallinity, as shown in Fig. A·1(c).

Polycrystalline samples of $\text{LaPt}_x\text{Si}_{2-x}$ ($x = 0.50, 0.75, 0.80, 0.85,$ and 1.00) were synthesized by arc-melting in an ultra-pure Ar atmosphere. Initially, high-purity elements La:Pt:Si (99.99% for La, and 99.999% for Pt and Si) were taken in ratios of $1:x:2-x$. The buttons were flipped and melted several times to ensure homogeneity. Subsequently, they were wrapped in Ta foil within a quartz ampoule and annealed at 950°C for 1 week. Cutting of both single crystals and polycrystals was performed using a wire electric discharge machine.

Appendix B: Single-crystal X-ray diffraction

Small pieces of single crystals were acquired by crushing a large single crystal, from which a crystal of dimensions $0.080 \times 0.062 \times 0.043 \text{ mm}^3$ was selected for single-crystal X-ray diffraction (SXRD) experiment at room temperature. SXRD was measured on a four-circle Bruker diffractometer employing $\text{Mo-K}\alpha$ (0.71073 \AA) radiation. Diffracted X-rays were detected by a Photon II detector where the crystal-to-detector distance was 50 mm, resulting in a resolution of the SXRD data of approximately $(\sin(\theta)/\lambda)_{\text{max}} = 0.694290 \text{ \AA}^{-1}$. See Table B·1 for the crystallographic information.

Appendix C: Electron-probe micro-analysis (EPMA)

Figure C·1 shows back scattered electron images of $x_{\text{nominal}} = 0.50, 0.75, 0.80, 0.85$. Points are labelled in the figure and analyzed. Table C·1 shows the results of the analysis. One observes a clear

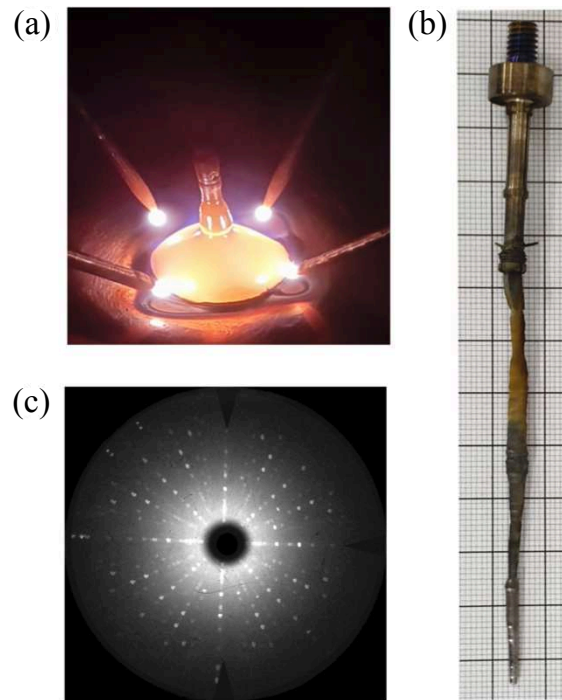


Fig. A-1. (Color online) (a) Crystal growth in a tetra arc furnace by the Czochralski method. (b) A cylindrical shaped ingot was obtained of about 70 mm in length and 4 mm in diameter. (c) Laue pattern corresponding to (001) plane suggesting a high quality single crystal.

phase separation for $x_{\text{nominal}} = 0.75, 0.80, \text{ and } 0.85$, while for $x_{\text{nominal}} = 0.5$ the phase is singular phase with minimal difference between x_{nominal} and x_{analyzed} .

Appendix D: Powder X-ray diffraction

Figure D-1 shows PXRD pattern of $\text{LaPt}_x\text{Si}_{2-x}$ with $x_{\text{nominal}} = 0.50, 0.75, 0.80, \text{ and } 0.85$. The diffraction pattern for $x_{\text{nominal}} = 0.50$ demonstrates the pure hexagonal phase, while the patterns for $x_{\text{nominal}} = 0.75, 0.80, \text{ and } 0.85$ exhibit both hexagonal and tetragonal diffractions. The peak intensities of hexagonal phase diminish with increasing Pt content x .

Table B.1. Crystallographic data of LaPt_{0.88}Si_{1.12}.

Temperature (K)	300
Crystal system	Tetragonal
Space group	<i>I4₁md</i>
Space group No.	109
<i>a</i> (Å)	4.2441(2)
<i>c</i> (Å)	14.5264(2)
Volume (Å ³)	261.66 (2)
<i>Z</i>	4
Wavelength (Å)	0.71073
Detector distance (mm)	50
θ -range (deg)	5.004 to 29.568
Rotation per image (deg)	0.5
$(\sin(\theta)/\lambda)_{\max}$ (Å ⁻¹)	0.694290
Absorption, μ (mm ⁻¹)	63.588
T _{min} , T _{max}	0.032, 0.102
Criterion of observability	$I > 3\sigma(I)$
Number of reflections	
measured	2777
unique (obs/all)	103/119
<i>R</i> _{int} (obs/all)	0.0620/0.0629
No. of parameters	15
<i>R</i> _F (obs)	0.0311
<i>wR</i> _F (all)	0.0509
GoF (obs/all)	3.67/3.49
$\Delta\rho_{\min}$, $\Delta\rho_{\max}$ (e Å ⁻³)	-3.95, 5.86

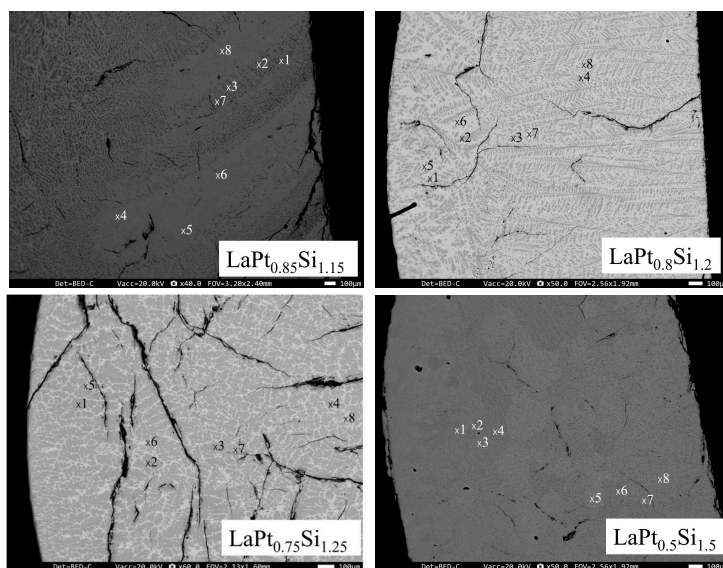


Fig. C-1. Back scattered electron images of $\text{LaPt}_x\text{Si}_{2-x}$ with $x_{\text{nominal}} = 0.50, 0.75, 0.80,$ and 0.85 .

Table C-1. Local composition x in $\text{LaPt}_x\text{Si}_{2-x}$ analyzed by EPMA for $x_{\text{nominal}} = 0.85, 0.80, 0.75,$ and 0.50 . Points measured are indicated in Fig. C-1.

Point no.	$\text{LaPt}_{0.85}\text{Si}_{1.15}$	$\text{LaPt}_{0.80}\text{Si}_{1.20}$	$\text{LaPt}_{0.75}\text{Si}_{1.25}$	$\text{LaPt}_{0.50}\text{Si}_{1.50}$
x1	0.709	0.694	0.697	0.499
x2	0.703	0.687	0.691	0.493
x3	0.709	0.697	0.695	0.492
x4	0.828	0.692	0.690	0.482
x5	0.821	0.859	0.870	0.478
x6	0.828	0.871	0.858	0.498
x7	0.820	0.867	0.873	0.501
x8	0.831	0.871	0.871	0.504

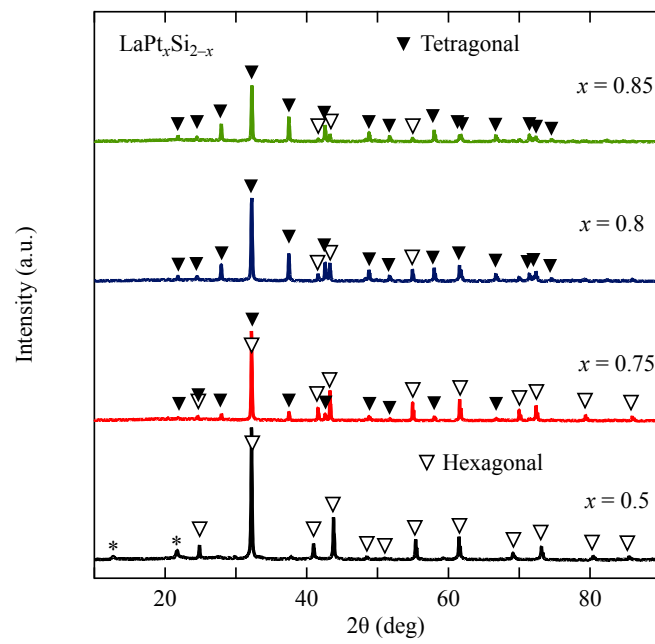


Fig. D-1. (Color online) PXRD pattern of $\text{LaPt}_x\text{Si}_{2-x}$ for $x_{\text{nominal}} = 0.50, 0.75, 0.80,$ and 0.85 . The filled and open triangles indicate the tetragonal and hexagonal peaks, respectively. Phase separation can be observed for all except for $x = 0.5$ where it is in the pure hexagonal phase.